

Interstellar Weather Vanes: GLIMPSE Mid-Infrared Stellar-Wind Bowshocks in M17 and RCW49

Matthew S. Povich^{1,5}, Robert A. Benjamin^{2,6}, Barbara A. Whitney³, Brian L. Babler¹, Rémy Indebetouw⁴, Marilyn R. Meade¹, and Ed Churchwell¹

ABSTRACT

We report the discovery of six infrared stellar-wind bowshocks in the Galactic massive star formation regions M17 and RCW49 from *Spitzer* GLIMPSE (Galactic Legacy Infrared Mid-Plane Survey Extraordinaire) images. The InfraRed Array Camera (IRAC) on the *Spitzer Space Telescope* clearly resolves the arc-shaped emission produced by the bowshocks. We combine *Two Micron All-Sky Survey* (*2MASS*), *Spitzer*, *MSX*, and *IRAS* observations to obtain the spectral energy distributions (SEDs) of the bowshocks and their individual driving stars. We use the stellar SEDs to estimate the spectral types of the three newly-identified O stars in RCW49 and one previously undiscovered O star in M17. One of the bowshocks in RCW49 reveals the presence of a large-scale flow of gas escaping the H II region at a few 10^2 km s⁻¹. Radiation-transfer modeling of the steep rise in the SED of this bowshock toward longer mid-infrared wavelengths indicates that the emission is coming principally from dust heated by the star driving the shock. The other 5 bowshocks occur where the stellar winds of O stars sweep up dust in the expanding H II regions.

Subject headings: infrared: ISM — shock waves — stars: winds — H II regions: individual(RCW49, M17)

¹Dept. of Astronomy, University of Wisconsin-Madison, 475 N. Charter St., Madison, WI 53706

²Dept. of Physics, University of Wisconsin-Whitewater, 800 W. Main St, Whitewater, WI 53190

³Space Science Institute, 3100 Marine Street, Suite A353, Boulder, CO 80303-1058

⁴Dept. of Astronomy, University of Virginia, Charlottesville, VA 22903-0818

⁵email: povich@astro.wisc.edu

⁶email: benjamin@wisp.physics.wisc.edu

1. Introduction

The Solar wind ends in a termination shock (e.g. Decker et al. 2005), where the pressure of the heliosphere balances the ram pressure of the surrounding interstellar medium (ISM). Massive stars with more energetic winds generate much stronger shocks. In cases where the relative motion between the star driving the wind and the ambient ISM is large, the shock will be bent back around the star. If the relative velocity is supersonic, the ambient ISM gas is swept into a second shock, forming an arc-shaped “bowshock” that is separated from the termination shock by a contact discontinuity. Stellar-wind bowshocks have been reported for a variety of sources, including nearby runaway O stars (van Buren & McCray 1988; van Buren, Noriega-Crespo, & Dgani 1995; Noriega-Crespo et al. 1997; Brown & Bomans 2005; Comerón & Pasquali 2007; France et al. 2007), high-mass X-ray binaries (Churchwell et al. 1992; Kaper et al. 1997; Huthoff & Kaper 2002), LL Ori-type stars (Bally et al. 2000), radio pulsars (Gaensler & Slane 2006), Galactic center O stars (Geballe et al. 2004, 2006), and mass-losing red giants (Martin et al. 2007). Recently, an infrared (IR) bowshock has been observed around the young A-type star δ Vel (Gáspár et al. 2008). Cometary H II regions also resemble bowshocks, due either to density gradients in the ambient gas or to motion of the ionizing source with respect to the interstellar surroundings (van Buren et al. 1990; Arthur & Hoare 2006). Both the direction of a bowshock and its “standoff distance” from the star generating the wind are determined by the velocity of the star with respect to the surrounding medium. In the case of runaway O stars, this is dominated by the high space motion of the star.

We report the detection of three mid-IR bowshocks in each of two massive star formation regions: M17 and RCW49. Two of the bowshocks in M17 are around known O stars. We will demonstrate that the other bowshocks are also around likely O stars. Since these stars are in or near expanding H II regions, we find that the direction of the bowshock is determined principally by the flow of the ISM rather than the space motion of the star.

2. Observations and Interpretation

The Galactic Legacy Infrared Mid-Plane Survey Extraordinaire (GLIMPSE; Benjamin et al. 2003) programs have mapped the inner Galactic midplane ($|l| \leq 65^\circ$) using the IRAC instrument on the *Spitzer Space Telescope* ($2''$ resolution; Fazio et al. 2004). RCW49, located at $(l, b) = (284.3, -0.3)$, was observed as part of the validation of the GLIMPSE observing strategy. The same area of the sky was imaged 10 times with 2-second exposures, and the combined data were mosaicked together to produce high resolution images ($0.6''$ pixels) of this region in the four IRAC bands: 3.6, 4.5, 5.8, and $8.0 \mu\text{m}$. An overview of these obser-

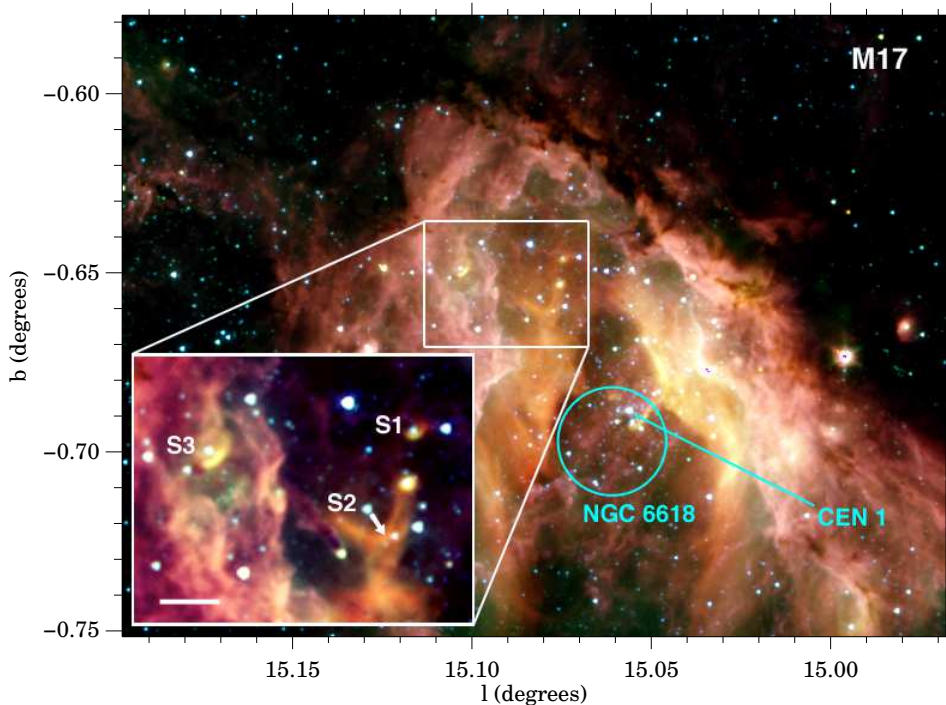


Fig. 1.— GLIMPSE full-color image of M17 (*blue*: $3.6 \mu\text{m}$, *green*: $4.5 \mu\text{m}$, *orange*: $5.8 \mu\text{m}$, *red*: $8.0 \mu\text{m}$). The region containing the bowshocks M17-S1, -S2, and -S3 is enlarged (scalebar shows $30'' = 0.23 \text{ pc}$ at 1.6 kpc). The central ring of O stars in the NGC 6618 cluster is circled. The bowshocks, along with the prominent pillar structure near M17-S2, all appear to be oriented in the general direction of CEN 1, the O4-O4 binary system in the center of the ionizing cluster.

variations was given by Churchwell et al. (2004). M17, at $(l, b) = (15.0, -0.7)$, was included in the GLIMPSE survey area, with two visits on the sky combined to make mosaics with $0.6''$ pixels.

2.1. M17

Povich et al. (2007) studied the diffuse emission morphology of M17 at multiple wavelengths from IR to radio, constraining the distance to $1.4\text{--}1.9 \text{ kpc}$. We will assume the widely-adopted value of 1.6 kpc for the M17 distance, following Nielbock et al. (2001). The winds and radiation of the O stars in the NGC 6618 cluster have excavated a cavity in the center of the M17 H II region. The cavity is filled with hot, X-ray-emitting gas from shocked stellar winds (Townsend et al. 2003). Povich et al. (2007) noted the presence of 3 appar-

ent stellar-wind bowshocks along the northern wall of the cavity, along with a prominent “elephant trunk,” or pillar, all oriented in the direction of the central ring of 7 O stars in NGC 6618. These structures are highlighted in Figure 1, a GLIMPSE image of M17 with an enlargement of the region containing the bowshocks. The bowshocks stand out as yellow-orange features in the image because they are faint at $3.6\ \mu\text{m}$ (colored *blue*) compared to the other 3 IRAC bands.

We designate these stellar-wind bowshocks in Figure 1 with the name of the region followed by an identification number, in order of increasing Galactic longitude (for example, M17-S1). IR fluxes for all of the bowshock driving stars are given in Table 1, and background-subtracted IR fluxes from aperture photometry of the bowshocks are listed in Table 2.

Spectral types of two of the driving stars have been determined photometrically (Bumgardner 1992) and spectroscopically (Hanson, Howarth, & Conti 1997). M17-S1 is associated with CEN 16, an O9–B2 star. The larger bowshock, M17-S2, is driven by CEN 18, an earlier-type star (O7–O8). Both bowshocks were detected at 10.5 and $20\ \mu\text{m}$ by Nielbock et al. (2001). These observations did not resolve the arc shapes of the bowshocks, and Nielbock et al. (2001) attributed the excess IR emission to circumstellar disks and classified CEN 16 and IRS 9 (the star visible just to the right of the arrowhead in Figure 1) as massive protostars.

M17-S3 lies outside of the field analyzed by Hanson, Howarth, & Conti (1997), and the driving star does not appear in any catalog of the region. It is not found in any GLIMPSE sourcelist, because the bright, spatially variable diffuse background prevented the automatic extraction of the point source. We measured the flux this source manually using a $5''$ aperture. Using the spectral energy distribution (SED) fitting tool of Robitaille et al. (2007), we fit the IR fluxes of this star (Table 1) with Kurucz (1993) stellar atmosphere models. Following the method described by Watson et al. (2008), we scale the models to the 1.6-kpc distance of M17 and estimate a spectral type of O7 V for the star. Carrying out the same analysis on 7 other O stars in M17 with independently known spectral types (Povich et al. 2008), we estimate that our spectral typing is accurate to within 2 subclasses.

2.2. RCW49

RCW49 presents a more complicated morphology than M17. Churchwell et al. (2004) discussed the structure and spectrum of the diffuse emission. Like M17, RCW49 is filled with X-ray gas (Townsend et al. 2005). The interstellar structures are dominated by two large cavities. The first, blown out to the West, contains the massive young cluster Westerlund 2, and the second is an enclosed bubble around the Wolf-Rayet star WR 20b (Figure 2). The

Table 1. 2MASS and IRAC^a IR Fluxes for Bowshock Driving Stars (mJy)

ID #	l	b	$F[J]$	$F[H]$	$F[K]$	$F[3.6]$	$F[4.5]^b$	$F[5.8]^b$
M17-S1	15.07486	-0.64607	196	214	186	96	67	...
M17-S2	15.08126	-0.65699	427	534	495	257	181	120
M17-S3 ^c	15.10325	-0.64867	103	200	238	151	≤ 154	≤ 155
RCW49-S1	284.07646	-0.43228	24	40	46	28	21	15
RCW49-S2	284.30107	-0.37121	10	18	20	13	≤ 11	≤ 27
RCW49-S3	284.33999	-0.28269	83	97	90	47	32	27

^aNone of these stars was detected in the IRAC [8.0] band.

^bIn cases where bowshock emission appears to cause a mid-IR excess over the stellar spectrum, the [4.5] and [5.8] fluxes are reported as upper limits. Due to suspected contamination from the bowshock or other diffuse emission, these fluxes are treated as upper limits to the stellar flux.

^cBecause the star driving SWB M17-3 is surrounded by bright, complex diffuse background emission, it was not extracted as part of the GLIMPSE point-source catalog. The fluxes reported here were measured using aperture photometry.

Table 2. IR Fluxes for Bowshocks (mJy)

ID #	l_{apex}	b_{apex}	IRAC Fluxes ^a			
			$F[3.6]^b$	$F[4.5]$	$F[5.8]$	$F[8.0]$
M17-S1	15.0744	-0.6465	≤ 34	71 ± 9	252 ± 42	1110 ± 290
M17-S2	15.0791	-0.6613	43 ± 17	245 ± 48	1240 ± 159	8700 ± 1500
M17-S3	15.1026	-0.6503	69 ± 16	240 ± 19	620 ± 100	1800 ± 320
RCW49-S1	284.0775	-0.4305	5.7 ± 0.9	12 ± 1	33 ± 1	322 ± 5
RCW49-S2	284.3018	-0.3712	≤ 2	9.6 ± 0.5	32 ± 3	172 ± 7
RCW49-S3	284.3388	-0.2829	≤ 21	50 ± 7	160 ± 20	825 ± 120
			<i>MSX</i> Fluxes ^c			
	MSXC6 Name		$F[8.3]$	$F[12.1]$	$F[14.6]$	$F[21.3]$
RCW49-S1	G284.0776-00.4340		627	2729	5674	1.56×10^4
			<i>IRAS</i> Fluxes ^c			
	<i>IRAS</i> Name		$F[12]$	$F[25]$	$F[60]$	$F[100]$
RCW49-S1	IRAS 10205-5729		3810	4.21×10^4	$\leq 2.26 \times 10^5$	2.75×10^5

^aThe IRAC fluxes are background-subtracted. Fluxes were measured using irregular apertures drawn to enclose all of the visible bowshock structure. Separate apertures were used to estimate the background flux. For each bowshock, the same set of apertures was used for all IRAC wavelengths.

^bIn cases where stellar emission appears to be confused with bowshock emission, the [3.6] bowshock fluxes reported are upper limits only.

^cRCW49-S1 is a point source in both the *MSX* and *IRAS* catalogs. All of the other bowshocks are confused with bright diffuse background IR emission features at the resolutions of *MSX* and *IRAS*.

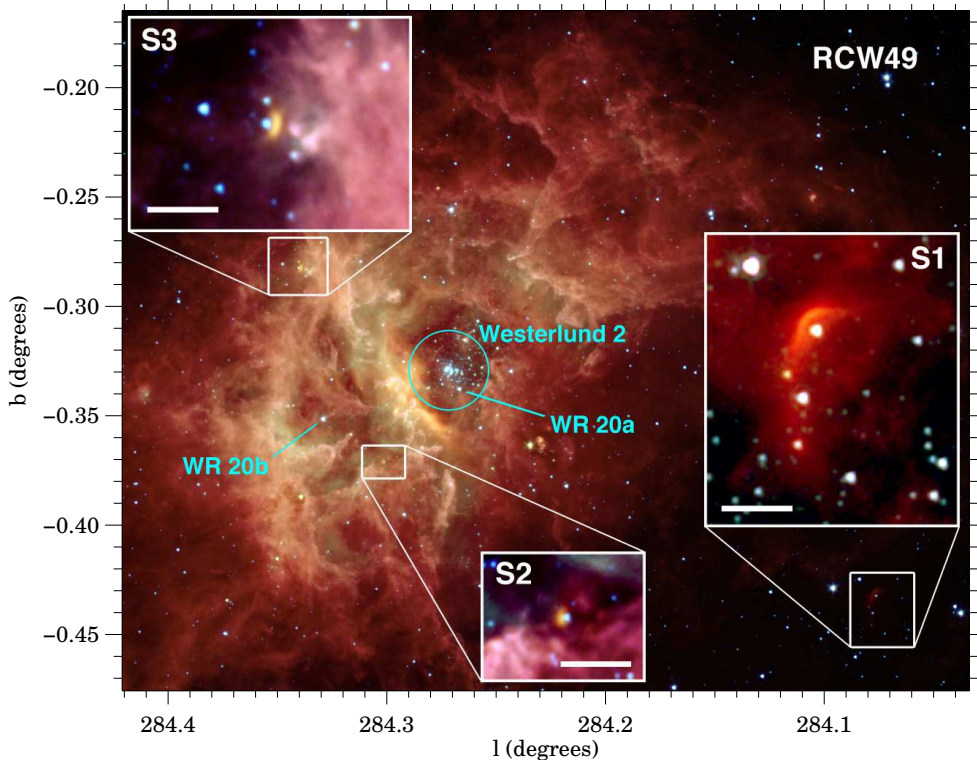


Fig. 2.— GLIMPSE full-color image of RCW49 (*blue*: [3.6], *green*: [4.5], *orange*: [5.8], *red*: [8.0]). The bowshocks RCW49-S1, -S2, and -S3, are enlarged in 3 separate insets (scalebars are $30'' \approx 0.6$ pc at 4.2 kpc). Three energy sources that could drive large-scale interstellar flows are also indicated: The Westerlund 2 cluster (circled), and the Wolf-Rayet stars WR 20a and WR 20b.

distance to RCW49 remains disputed, with recent estimates placing the region as close as 2.8 kpc (Ascenso et al. 2007) or as far as 8.0 kpc (Rauw et al. 2007), with a kinematic distance estimate of 6 ± 1 kpc (Dame 2007). We consider distances of both 4.2 kpc (Churchwell et al. 2004) and 6 kpc in our analysis.

We have found three bowshocks associated with RCW49, shown in three separate insets in Figure 2. RCW49-S1 is unique among our sample, because it lies relatively far from the H II region, but we believe it is associated with RCW49 for the following reasons: (1) The RCW49 distance is consistent with the luminosity of the driving star being an O star (see below); and (2) the bowshock points (approximately) toward the central cluster, Westerlund 2. Because it is far from any other bright IR source, RCW49-S1 appears as a point source in both the *Midcourse Space Experiment* (MSX; Price et al. 2001) and *Infrared Astronomical Satellite* (IRAS; Beichman et al. 1988) point source catalogs, and these fluxes are also given

in Table 2.

RCW49-S2 is oriented away from Westerlund 2 and appears to be influenced primarily by the nearby WR 20b. RCW49-S3 is oriented in the general direction of Westerlund 2. None of the RCW49 bowshocks points directly back toward the central cluster, while all three M17 bowshocks do. Perhaps the expanding bubbles driven by Westerlund 2 and the Wolf-Rayet stars are interacting turbulently, producing non-radial components to the flows. It is also possible that the bowshock driving stars have large orbital motions relative to the dynamic interstellar medium.

The three bowshock driving stars in RCW49 are of previously undetermined spectral type, so we again estimate the spectral type by fitting model SEDs to the broadband fluxes of Table 1, scaled to both the 4.2 kpc and 6 kpc distances. The results are given in Table 3. [ht]

All three stars are plausibly O stars. Assuming 4.2 kpc, the driving star of RCW49-S1 is fit as O6 V, RCW49-S2 as O 9 V, and RCW49-S3 as O5 V (or O9 III). If we increase the distance to 6 kpc, the fits become O 5 III, O6 V, and O5 V (or O6.5 III), respectively (see Watson et al. 2008, for an explanation of the degeneracy between luminosity classes). The spectral types at 6 kpc seem improbably luminous. Highly luminous and windy stars dominate the dynamics of their local ISM. We do not observe IR bowshocks around any of the earliest-type stars in either RCW49 or M17, because they have blown large, evacuated cavities in the centers of the H II regions. Little or no ambient material remains close to the stars to produce a bowshock.

Apart from the Wolf-Rayet systems, one of the earliest stars in RCW49 is G284.2642-00.3156. Using optical spectroscopy, Uzpen et al. (2005) classified this star as O4 V(f) and derived a spectrophotometric distance of 3.2 ± 0.5 kpc. Using IR SED fitting, we confirm that the luminosity of this star is consistent with an O4 V star at 3.2 kpc. Yet this distance falls on the low end of the range of published distance estimates for RCW49, and we do not adopt it here. Like CEN 1 in M17, G284.2642-00.3156 may be an unresolved, equal-mass O4–O4 binary. Doubling the luminosity moves the spectrophotometric distance from 3.2 to 4.5 kpc, in agreement with a distance of 4.2 kpc but inconsistent with 6 kpc.

3. Bowshock Properties

The standoff distance d_w of a bowshock from its driving star is the point where the momentum flux of the stellar wind balances the momentum flux of the ambient medium: $n_w v_w^2 = n_0 v_0^2$. Following van Buren & McCray (1988), we normalize the stellar wind mass

Table 3. Bowshock Standoff Distances and Estimated Stellar Wind Properties

ID #	Spectral type ^a	$\dot{M}_{w,-6} v_{w,8}$ ^b	$d_w \cos i$ (pc)	$d_{cl} \cos i$ (pc)	$v_0 n_{0,3}^{1/2} (\cos i)^{-1}$ (km s ⁻¹)
M17 Distance = 1.6 kpc					
M17-S1	O9–B2 V	≤ 0.2	0.03	1.4	≤ 22
M17-S2	O7–O8 V	0.5–2.5	0.11	0.9	10–22
M17-S3	O7 V	0.5–2.5	0.05	1.7	21–47
RCW49 Distance = 4.2 kpc					
RCW49-S1	O6 V	~ 1.3	0.16	16.2	11
RCW49-S2	O9 V	~ 0.2	0.04	2.46	17
RCW49-S3	O5 V or O9 III	2.5–3.2	0.096	6.13	25–28
RCW49 Distance = 6.1 kpc					
RCW49-S1	O5 III	~ 16	0.23	23.2	26
RCW49-S2	O6 V	~ 1.3	0.06	3.52	28
RCW49-S3	O3 V or O6.5 III	> 3.2	0.14	8.8	> 19

^aSpectral types for the stars driving M17-S1 and -S2 are taken from CEN and Hanson, Howarth, & Conti (1997). All others were estimated by fitting Kurucz (1993) stellar atmosphere models to the broadband IR fluxes (Table 1) and scaling to the distance of M17 or RCW49. Spectral types given for RCW49 are highly uncertain due to the disputed distance to that region.

^bEstimates of stellar mass-loss rates $\dot{M}_{w,-6} = \dot{M}_w / (10^{-6} M_\odot \text{ yr}^{-1})$ and wind velocities $v_{w,8} = v_w / (10^8 \text{ cm s}^{-1})$ are based upon Vink, de Koter, & Lamers (2001) and Fullerton, Massa, & Prinja (2006).

loss rate, $\dot{M}_{w,-6} = 10^{-6} M_{\odot} \text{ yr}^{-1}$, stellar wind velocity $v_{w,8} = 10^8 \text{ cm s}^{-1}$, ambient hydrogen particle density of $n_{0,3} = 10^3 \text{ cm}^{-3}$, and use a mean ISM gas mass per hydrogen atom $\mu = 2.36 \times 10^{-24} \text{ g}$. Assuming a spherically symmetric stellar wind with a mass-loss rate given by $\dot{M} = 4\pi d_w^2 \mu n_w v_w$, the velocity of the star with respect to the ambient ISM can be written as

$$v_0 = 1.5 \left(\frac{d_w}{\text{pc}} \right)^{-1} (\dot{M}_{w,-6} v_{w,8})^{1/2} n_{0,3}^{-1/2} [\text{km s}^{-1}], \quad (1)$$

where v_w is the terminal velocity of the stellar wind. Values of $v_0 n_{0,3}^{1/2}$ and d_w for each bowshock are presented in Table 3. The standoff distance can be measured only as $d_w \cos i$ on the sky, where i is the inclination (or viewing angle) made by the line connecting the star with the apex of the bowshock against the plane of the sky ($i = 0$ if the line joining the star to the bowshock apex lies in the plane of the sky). Because a bowshock oriented at high i will not produce an arc morphology, it is likely that $i \lesssim 45^\circ$, and hence $\cos i$ will not differ greatly from unity in our measurements.¹ The distance from each bowshock to the likely source of the large-scale ISM flow, measured on the sky as $d_{cl} \cos i$, are also presented for reference in Table 3.

The mass-loss rates and stellar wind velocities in Equation 1 suffer from high dispersion as a function of spectral type (Fullerton, Massa, & Prinja 2006), a factor of 2 or even greater, and this is compounded by a comparable level of uncertainty in the spectral types. The uncertainty on our measurements of d_w ranges from $\sim 20\%$ for the largest bowshocks (M17-S2 and RCW49-S1) to $\sim 40\%$ for the smaller bowshocks that are barely resolved by IRAC. We estimate that $v_0 n_0^{1/2}$ is uncertain by a factor of 2 in M17 and up to a factor of 3 in RCW49, where the spectral types of the driving stars are less constrained. These uncertainties, reflected in the range of values for $v_0 n_0^{1/2}$ in Table 3, are dominated by the uncertainty in the stellar wind properties.

We have neglected the effects of turbulent pressure in our calculation of the momentum flux balance of the bowshocks. This is a potentially significant contributor to the total ISM pressure held off by the bowshocks. The effect of turbulent pressure would be to systematically decrease the standoff distance d_w , causing us to overestimate v_0 .

In reality, for the fast winds of early-type stars, the observed bowshock is displaced from the standoff distance by a significant amount. This happens because the cooling timescale of the shocked stellar wind is very long. The result is a thick layer of hot gas intervening between the wind terminal shock at the standoff distance and the thin, dense layer of interstellar gas and dust forming the observed bowshock. The numerical simulations of Comerón & Kaper

¹The average value of $\cos i$ for $0 \leq i \leq 45^\circ$ is 0.9.

(1998) predict that the bowshock should be located at twice the standoff distance from the driving star. In this case, our derived values of $v_0 n_0^{1/2}$ in Table 3 would be underestimated by the same factor of 2. This systematic correction is comparable to the intrinsic uncertainties in our estimates of $v_0 n_0^{1/2}$, and it partially compensates for the effects of neglecting turbulent pressure in the ambient ISM. Therefore, the assumption that the observed distance of the bowshocks from the driving stars corresponds to the standoff distance d_w should not have a large impact on our results, and we find that the cautious application of Equation 1 yields reasonable results.

Orbital velocities of O stars in massive clusters are typically $< 10 \text{ km s}^{-1}$. The expansion speed of ionized gas in H II regions is generally comparable to the sound speed of $\sim 10 \text{ km s}^{-1}$, and this appears to be true in M17 (Pellegrini et al. 2007). Most of the bowshocks (the exception being RCW49-S1) are apparently located within the ionized gas of the radio H II regions. The likely explanation for the bowshock emission in the IR is that dust in the H II regions (Povich et al. 2007) is swept-up by the bowshocks. The observed average electron density in the Northern bar of the M17 H II region is $\sim 10^3 \text{ cm}^{-3}$ (Felli, Churchwell, & Massi 1984), so the values of $v_0 n_{0,3}^{1/2}$ listed in Table 3 are likely to be close to the actual relative velocities of the stars and the ISM for most of the bowshocks.

The values of $v_0 n_{0,3}^{1/2}$ calculated for M17-S1 and -S2 are in good agreement. M17-S3, however, presents a different picture. M17-S3 appears to be associated with a “teardrop” structure (Figure 1) in the photodissociation region (PDR), near the ionization front. The ambient density surrounding this star could be significantly higher than the density within the H II region. If v_0 for this bowshock is comparable to that of the other 2 bowshocks in M17, then $n_{0,3} \sim 2.25 \text{ cm}^{-3}$ in this location. This value agrees with the measurements of electron density in the dense clumps of ionized gas in M17 (Felli, Churchwell, & Massi 1984). The unusual morphology of the diffuse IR emission associated with M17-S3 suggests that the star may have recently emerged from an evaporating globule on the edge of the PDR; a larger, more evolved analog of the nearby pillar structure seen in Figure 1.

In RCW49, all 3 bowshocks are found in very different locations, but we note that 2 of the bowshocks appear to be similar in size, color, and ambient environment (Figure 2). The largest bowshock, RCW49-S1, is different, since it is located relatively far (16.2 pc at 4.2 kpc) from Westerlund 2, outside the H II region. The presence of RCW49-S1, along with its orientation, indicates that RCW49 vents a large-scale flow of gas through the cavity opening to the West. This flow likely originates in the combined winds of the Westerlund 2 cluster and thus should be much more diffuse than the H II region gas (Townsend et al. 2003, 2005). Assuming a density of 1 cm^{-3} in the flow from Westerlund 2, the standoff distance of RCW49-S1 at 4.2 kpc gives a flow velocity of $\sim 350 \text{ km s}^{-1}$. Such a high value of v_0 is

reasonable, given that the gas must move supersonically relative to the star to produce a shock, and the sound speed in the hot, rarefied gas of the flow streaming away from the H II region is $\sim 100 \text{ km s}^{-1}$.

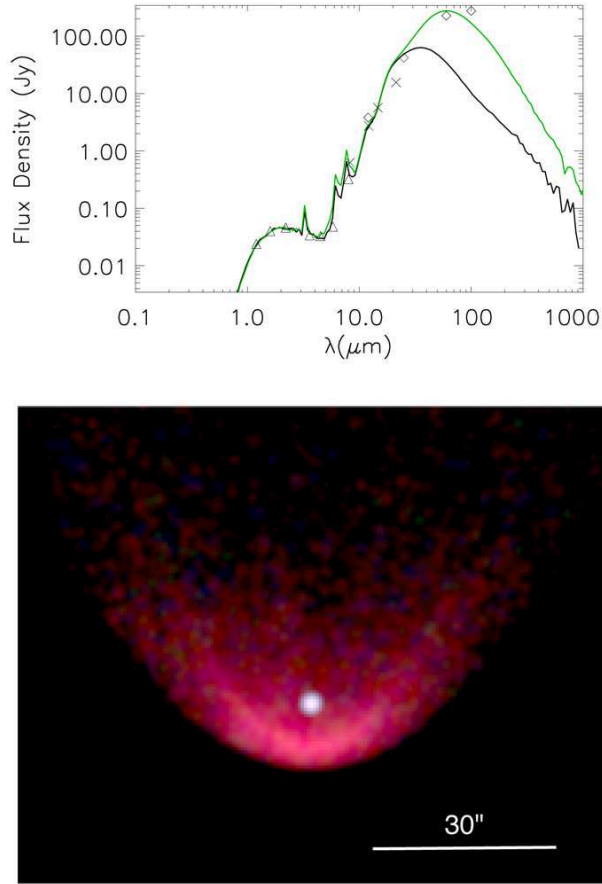


Fig. 3.— Radiation transfer model of RCW49-S1. *Top*: Model SEDs plotted with the fluxes of the bowshock and driving star from Tables 1 & 2 (*triangles*: 2MASS and GLIMPSE; *crosses*: MSX; *diamonds*: IRAS). The *green* curve includes low-density material in a shell 2–3 pc from the star in order to match the IRAS 60 and 100 μm fluxes. *Bottom*: Image of the model bowshock at GLIMPSE wavelengths (compare to Fig. 2).

Because RCW49-S1 was detected by MSX and IRAS in addition to GLIMPSE, we can construct the SED of the bowshock from 4.5 μm to 100 μm (Table 2). We computed SED models of RCW49-S1 using a 3-D radiative equilibrium code (Whitney et al. 2003) modified to include very small grain (VSG) and PAH emission (Wood et al. 2008). We used the canonical mass fraction for VSG/PAH grains of 5% (Draine & Li 2007). We modeled the bowshock geometry as a paraboloid with the apex offset by $d_w = 0.16 \text{ pc}$ from the O6 V star

(assuming $i = 0$ and the 4.2 kpc distance). For models that reproduced the observed images, the SED shape was insensitive both to the thickness of the shock and to the radial density profile of the dust (with the total mass scaled to match the observed SED). The black line in Figure 3 shows the SED for a model with a density varying as r^{-2} from the 0.16 pc standoff distance out to a radius of 1.5 pc. The observed SED shortward of $30 \mu\text{m}$ is well-matched by the model. For radial density exponents from -2 to 0 , the mass of this material ranges from $\sim 0.5 M_{\odot}$ to $2 M_{\odot}$, respectively, assuming a dust-to-gas mass ratio of 0.01. The optical depth in all models is low, with $A_V < 0.02$ within 1 pc. To match the *IRAS* data at 60 and $100 \mu\text{m}$ requires low-density material farther from the star. The *green* line in Figure 3 is a model including a shell 2–3 pc from the star. This material added mid-IR PAH emission, so we lowered the VSG/PAH mass fraction to 3% to continue to match the mid-IR SED, and the image still matches the data well. The A_V through the bowshock in this model is 0.25, most of it due to the outer shell. Along the line of sight to the star, $A_V = 10$, so the bowshock and shell contribute a negligible fraction of the interstellar extinction. These models show that dust distributed in a bowshock geometry matches both the images and the SED reasonably well. The IR emission from the bowshock can be explained by reprocessed stellar radiation without any additional dust heating by the shock.

The structure of RCW-S1 is probably significantly different from that of the other 5 bowshocks in our sample, because it is located in a distinct interstellar environment. Because of the high temperature and low density in the flow outside the H II region, the shocked interstellar gas cannot cool quickly enough to form a dense layer behind the bowshock, as likely happens in the other 5 cases. The shock is approximately adiabatic, remaining very hot and only moderately compressed (by a factor of ~ 4) as it flows past the star, forming a relatively thick layer. Hence, while RCW-S1 is the only bowshock in our sample observed at enough different mid-IR wavelengths to allow us to create a meaningful model of the emission, it may not be appropriate to draw strong conclusions about the remaining bowshocks based upon this model.

4. Summary

We have observed 6 prominent IR bowshocks in M17 and RCW49. These objects appear to be produced by the winds of individual O stars colliding with large-scale interstellar gas flows in the H II regions. One bowshock, M17-S3, may be the leading edge of an evaporating globule containing a newly-formed and previously undiscovered O star in the well-studied M17 region. All three bowshocks associated with RCW49 lead us to identify new candidate O stars. Our stellar classifications also suggest that the true distance to RCW49 is less than

the kinematic distance of 6 kpc.

The bowshocks are bright at IR wavelengths due to emission from dust swept up from the ambient ISM and heated by radiation from the bowshock driving stars. As Gáspár et al. (2008) note, IR excess emission from a bowshock could be attributed to the presence of a circumstellar disk, particularly when the bowshock morphology is not spatially well-resolved. This can be a pitfall for observational studies of accreting massive protostars.

The collective winds of the most luminous stars in young, massive clusters produce overlapping large-scale flows that hollow out thermally hot cavities in the parent molecular cloud (Townesley et al. 2003). The largest bowshock presented here, RCW49-S1, is evidence that the combined winds of the ionizing stars in Westerlund 2 have escaped the H II region, creating a flow of hot gas moving at a few 10^2 km s⁻¹ that extends at least 16 pc away from RCW49.

The driving stars of the other 5 bowshocks are surrounded by ionized gas and dust of their natal H II regions, where the density of the ambient medium ($n_0 \sim 10^3$ cm⁻³) is sufficiently high to produce the observed bowshocks with a relative velocity of only 10–20 km s⁻¹. The winds of the bowshock driving stars do not directly encounter the >2000 km s⁻¹ winds from the most massive stars in the cluster. Instead, the bowshocks are shaped by the expansion of the ionized gas in the H II regions relative to the orbital motions of the stars.

Eventually, supernova explosions will produce high velocity shock waves that heat and disperse the original gas cloud. In star forming regions like M17 and RCW49 that have not yet been disrupted by supernovae, IR bowshocks serve as interstellar “weather vanes,” indicating the speed and direction of large-scale gas flows at points within and around giant H II regions.

We thank the anonymous referee for incisive and very useful suggestions that helped us improve this work. We are grateful to Joseph Cassinelli, Eric Pellegrini, John Raymond, Ellen Zweibel, Heidi Gneiser, and Don Cox for useful conversations while preparing this paper. M. S. P. thanks the members of the “dissertator club,” Kathryn Devine, K. Tabetta Hole, and Nicholas Murphy, for their helpful comments. This work was supported by NSF grant AST-030368 (E. B. C.) and NASA/JPL Contracts 1282620 and 1298148. Additional support was provided by the NASA Theory Program (NNG05GH35G; B. A. W.). R. I. acknowledges support from a Spitzer Fellowship at the time that these data were analyzed, and from JPL RSA1275467.

REFERENCES

- Arthur, S. J., & Hoare, M. G. 2006, *ApJS*, 165, 283
- Ascenso, J., Alves, J., Beletsky, Y., & Lago, M. T. V. T. 2007, *A&A*, 466, 137
- Bally, J., O'Dell, C. R., & McCaughrean, M. J. 2000, *AJ*, 119, 2919
- Beichman, C. A., Neugebauer, G., Habing, H. J., Clegg, P. E., & Chester, T. J., eds. 1988, *IRAS Catalogs and Atlases: Explanatory Supplement*, NASA RP-1190
- Benjamin, R.A. et al. 2003, *PASP*, 115, 953
- Brown, D., & Bomans, D. J. 2005, *A&A*, 439, 183
- Bumgardner, T. E. 1992, M.S. thesis, Ohio State Univ., Columbus
- Chini, R., Elsässer, H., & Neckel, T. 1980, *A&A*, 91, 186 (CEN)
- Churchwell, E., Bieging, J. H., van der Hucht, K. A., Williams, P. M., Spoelstra, T. A. Th., & Abbott, D. C. 1992, *ApJ*, 393, 329
- Churchwell, E. et al. 2004, *ApJS*, 154, 322
- Comerón, F. & Kaper, L. 1998, *A&A*, 338, 273
- Comerón, F. & Pasquali, A. 2007, *A&A*, 467, L23
- Dame, T. M. 2007, *ApJ*, 665, L163
- Decker, R. B. et al. 2005, *Science*, 309, 2020
- Draine, B. T. & Li, A. 2007, *ApJ*, 657, 810
- Fazio, G. G. et al. 2004, *ApJS*, 154, 10
- Felli, M., Churchwell, E., & Massi, M. 1984, *A&A*, 136, 53
- France, K., McCandliss, S. R., & Lupu, R. E. 2007, *ApJ*, 655, 920
- Fullerton, A. W., Massa, D. L., & Prinja, R. K. 2006, *ApJ*, 637, 1025
- Gaensler, B. M., & Slane, P. O. 2006, *ARA&A*, 44, 17
- Gáspár, A., Su, K. Y. L., Rieke, G. H., Balog, Z., Kamp, I., Martínex-Galarza, J. R., & Stapelfeldt, K. 2008, *ApJ*, 672, 974

- Geballe, T.R., Rigaut, F., Roy, J.-R., & Draine, B.T. 2004, *ApJ*, 602, 77
- Geballe, T. R., Najarro, F., Rigaut, F., & Roy, J.-R. 2006, *ApJ*, 652, 370
- Hanson, M. M., Howarth, I. D., & Conti, P. S. 1997, *ApJ*, 489, 698
- Huthoff, F., & Kaper, L. 2002, *A&A*, 383, 999
- Kaper, L., van Loon, J. T., Augusteyn, T., Goudfrooij, P., Patat, F., Waters, L. B. F. M., & Zijlstra, A. A. 1997, *ApJ*, 475, L37
- Kurucz, R. 1993, ATLAS9 Stellar Atmosphere Programs and 2 km/s grid. Kurucz CD-ROM No. 13. Cambridge, MA: Smithsonian Astrophysical Observatory
- Martin, D, C. et al , 2007, *Nature*, 448, 780
- Nielbock, M., Chini, R., Jütte, M., & Manthey, E. 2001, *A&A*, 273, 284
- Noriega-Crespo, A., van Buren, D., & Dgani, R. 1997, *AJ*, 113, 780
- Pellegrini, E. W. et al. 2007, *ApJ*, 658, 1119
- Povich, M. S., Stone, J. M., Churchwell, E., Zweibel, E. G., Wolfire, M. G., Babler, B. L., Indebetouw, R., Meade, M. R., & Whitney, B. A. 2007, *ApJ*, 660, 346
- Povich, M. S. et al. 2008, *ApJ*, submitted
- Price, S. D., Egan, M. P., Carey, S. J., Mizuno, D. R., and Kuchar, T. A. 2001, *AJ*, 121, 2842
- Rauw, G., Manfroid, J., Gosset, E., Nazé, Y., Sana, H., De Becker, M., Foellmi, C., & Moffat, A. F. J. 2007, *A&A*, 463, 981
- Robitaille, T. P., Whitney, B. A., Indebetouw, R., & Wood, K. 2007, *ApJS*, 169, 328
- Townsley, L. K., Feigelson, E. D., Montmerle, T., Broos, P. S., Chu, Y.-H., & Garmire, G. P. 2003, *ApJ*, 593, 874
- Townsley, L., Feigelson, E., Montmerle, T., Broos, P., Chu, Y.-H. Garmire, G., & Getman, K. 2005, *X-Ray and Radio Connections*, eds. L.O. Sjouwerman & K.K Dyer (NRAO: Santa Fe, NM)
- Uzpen, B. et al. 2005, *ApJ*, 629, 512
- van Buren, D. & McCray, R. 1988, *ApJ*, 329, 93

- van Buren, D., Mac Low, M. M., Wood, D. O. S., & Churchwell, E. 1990, *ApJ*, 353, 570
- van Buren, D., Noriega-Crespo, A., & Dgani, R. 1995, *AJ*, 110, 2914
- Vink, J. S., de Koter, A., & Lamers, H. J. G. L. M. 2001, *A&A*, 369, 574
- Watson, C., Povich, M. S., Churchwell, E. B., Babler, B. L., Chunev, G. Hoare, M., Indebetouw, R., Meade, M. R., & Whitney, B. A. 2008, *ApJ*, 681, 1341 (astro-ph 0806.0609)
- Whitney, B. A., Wood, K., Bjorkman, J. E., & Wolff, M. J. 2003, *ApJ*, 591, 1049
- Wood, K., Whitney, B. A., Robitaille, T. P., & Draine, B. T. 2008, *ApJ*, in press (astro-ph 0807.2398)